Korean J. Chem. Eng., 35(3), 784-791 (2018)
DOI: 10.1007/s11814-017-0314-8

pISSN: 0256-1115
eISSN: 1975-7220

Tramadol hydrochloride delivery by regenerated cellulose nanofiber-TiO_2-ZnO composites

Gabriel Ademola Olatunji*, Adeola Tawakalt Kola-Mustapha, Oluwaseyi Damilare Saliu*,†, Aderemi Babatunde Alabi***, Oluwafemi Idowu Abiodun*, and Nike Olatayo Obisesan***

*Department of Industrial Chemistry, University of Ilorin, Ilorin, Nigeria
**Department of Pharmaceutics and Industrial Pharmacy, University of Ilorin, Ilorin, Nigeria
***Department of Physics, University of Ilorin, Ilorin, Nigeria
(*Received 28 April 2017 • accepted 20 November 2017*)

Abstract−The present work focuses on the development and investigation of new composite materials based on regenerated nanocellulose, titanium oxide (TiO_2) and zinc oxide (ZnO) with potentials for drug delivery applications. The new composite was developed using dispersion method. The physicochemical properties of the composites were extensively evaluated using scanning electron microscopy (SEM), X-ray diffraction (XRD), particle size analyzer and Fourier transform infrared spectroscopy (FTIR). The presence of O-H, C-H, C-O-C, Ti-O, Zn-O stretch and bend was confirmed using the FTIR, while the SEM revealed the TiO_2 and ZnO immobilized on the surface of stiff and rod-like strands of regenerated nanocellulose. The XRD showed characteristic peaks at 2θ of 16.6°, 22.7°, 34.4° for nanocellulose, 17.5°, 24.5°, 32° for ZnO and 25.4°, 38°, 48.3°, 53.8° for TiO_2. As the amount of the metal oxides in the composite increased, notable increase in physicochemical properties and morphology for drug delivery purpose was observed. The cumulative drug release profiles of the regenerated nanocellulose composites on tramadol hydrochloride were subjected to zero order, first-order, Higuchi and Korsmeyer-Peppas plots, and fitted most for Korsmeyer-Peppas with R^2 and n value from 0.9831 to 0.9941 and 0.4188 to 0.9704, respectively.

Keywords: Regenerated, Nanocellulose, Zinc Oxide, Titanium Oxide, Composite

INTRODUCTION

Some of the most recent applications of cellulosic material include the industrial production of paper, coatings, laminates, optical films and sorption media; composites of inorganic metal oxides for photocatalysis, drug delivery, and antibacterial agents [1]. The high strength and network structure of cellulose fibers coupled with biocompatibility, biodegradability and surface morphology provide opportunities to study and incorporate this biomaterial into the future material needs in medicine, pharmaceuticals, cosmetics, electronics and energy industries. The biocompatibility property makes this biopolymer qualify for health applications such as wound healing, burn dressing, tissue regeneration applications and controlled drug release or delivery applications [2].

The main advantages of nanoscaled titania are its long-term chemical stability when exposed to acidic and basic media, nontoxicity, its high biocompatibility and relatively low cost [3,4]. TiO_2 can be used for self-sterilization, as self-cleaning surface, photochromic, super hydrophobic and hydrophilic coatings, matrices for bioencapsulation, drug delivery and tissue engineering [5]. Zinc oxide (ZnO) is an important basic material due to its low cost, large band gap, and luminescent properties. It is widely used in many applications such as catalyst, gas sensors, filtering materials for ultraviolet light, transparent conductive oxide, in painting industry and in reduction of germs, virus, and algae by oligodynamic effect of metal oxide component.

Nanocellulosic papers formed from nanofibrillated cellulose and zinc oxide composite with bacteriostatic and bactericidal activities are used as fillers in starch based coating formulations [6]. Also, cellulose nanocrystals and zinc oxide have proved to increase the tensile strength and modulus of poly (vinyl alcohol) and chitosan film after blending by a solvent casting method from 55.0 to 153.2 MPa and from 395 to 932 MPa, respectively, with increasing nanosized filler amount from 0 to 5.0 wt% [7]. Various cellulosic nanoparticles and acid corroded titanium oxide nanobelts composites having photocatalytic activity have been used to degrade methylene blue, rhodamine and other organic pollutants in aqueous solution. Silver and gold-doped nanocellulose and titania hybrid films show high antimicrobial properties under ultraviolet radiation exposure [8].

The development of new functional biopolymer metal oxides is experiencing a tremendous increase in research activity because this new form of smart material combines the special properties of biodegradability, biocompatibility and high surface area of cellulosic materials with that of inorganic materials. Regenerated nanocellulose/TiO_2/ZnO hybrid permits the extension of the major application of cellulosic polymer materials for drug release or delivery, biological activity, photocatalysis, and highly enhanced antibacterial properties [5]. Therefore, cellulose alone with its limited physical properties which cannot satisfy this wide range of applications can now be functionalized by incorporating nano, micro and

†To whom correspondence should be addressed.
E-mail: oluwaseyi229@gmail.com
Copyright by The Korean Institute of Chemical Engineers.

sub-micron inorganic materials depending on the end applications [4].

Tramadol hydrochloride is generally used in the treatment of osteoarthritis, diabetic neuropathy, clinical pains and other forms of body pains. It is a form of opioid analgesic which acts on the central nervous system by binding to the opioid receptors for the release of serotonin and the inhibition of the re-uptake of norepinephrine [9]. Tramadol hydrochloride, which is a free soluble drug in water, has a half-life of about 5.5 hours and its usual dosage is around 60 to 90 mg every 4 to 6 hours [10]. Therefore, a swellable hydrogel matrix is needed for its sustained release not only to improve patients' compliance and decrease habit forming, but to increase the input rate of the drug in patients by careful optimization of the hydrophobic content of swellable polymer composite matrix for its delivery [11]. This research work is aimed at the delivery of tramadol hydrochloride using regenerated nanocellulose and hydrophilic metal oxide composites.

MATERIALS AND METHOD

1. Materials

Isoberlinia doka (Yoruba: Ayin) wood dust was obtained from Tanke Sawmill, Tanke Ilorin, Kwara state, Nigeria. TiO_2 and ZnO were obtained from Sigma Aldrich, UK. NaOH (16%), n-hexane, toluene, ethanol, HNO_3, H_2SO_4, sodium hypochlorite, H_2O_2 (6%), acetic acid, urea, phthalic anhydride and adipic acid were obtained from BDH Analar, England. The special apparatus used included a pycnometer, ultrasonicator, hot plate/magnetic stirrer, and nano filter pump.

2. Chemical Treatment of the Wood Dust

The method of Chauhan et al. (2009) was adopted. The wood dust was placed in hot water-steam for about 10 minutes, allowed to cool and filtered. 15% NaOH and 6% H_2O_2 was added to the wood dust (4 : 1 liquor to biomass ratio) and heated for 90 minutes [11].

3. Delignification of the Lignocellulose

The acid chlorite treatment method was modified. The lignocellulose was soaked in distilled water before being treated with 20% of HNO_3 in ethanol. Sodium chlorite and glacial acetic acid were later added and the mixture was heated in a water bath at 70 °C. The pulp sample was subjected to three cycles every two hours.

4. Preparation of Regenerated Cellulose Nanofiber

The cellulosic material was dissolved in 8% NaOH and 12% urea at a temperature range of −1 to −5 °C. The mixture was properly stirred for at least 10 minutes. This was repeated two times before regenerating the cellulose in 50% H_2SO_4. The regenerated nanocellulose was filtered using a nano pump, washed with ethanol and the size was evaluated using particle size analyzer [12,13].

5. Preparation of TiO_2 and ZnO Dispersion

The method used by Snyder and Schutz was adopted with some modification. A stock dispersion of TiO_2 and ZnO was prepared by dispersing TiO_2 and ZnO in 0.1 M HCl through a combination of mechanical mixing and sonication [6,8].

6. Preparation of Regenerated Nanocellulose, TiO_2 and ZnO Composite

The regenerated nanocellulose was crosslinked by dispersing it in a mixture of adipic acid and glycerol at 70 °C and stirred for one hour. The composites were prepared by mixing the crosslinked regenerated nanocellulose with varying amounts of TiO_2 and ZnO in 5% HCl. The dispersions containing different ratios of TiO_2 and ZnO were shaken for 2 hours and the pH was adjusted to 8 with aqueous solutions of diluted ammonia. The composites were dried at 40 °C in an oven [12].

Table 1. The composition of each regenerated nanocellulose composite

Composites	Regenerated nanocellulose (RNC) (%)	Zinc oxide (%)	Titanium oxide (%)
RNCC1	98	1	1
RNCC2	96	2	2
RNCC3	94	3	3
RNCC4	92	4	4
RNCC5	90	5	5

Table 1 above shows the composition of zinc oxide and titanium oxide in 10.0 g of each composite. The regenerated nanocellulose in the composite ranged from 9.0 to 9.8 g, while the metallic oxides (TiO_2 and ZnO) composited with it ranged from 0.1 to 1.0 g.

7. Hydration (Swelling) Studies

We investigated the maximum time required for the microspheres to completely hydrate and their maximum swelling capacity in phosphate buffer solution. The buffer was prepared by the addition of 100 mL of KH_2SO_4 (0.1 M) to 13 mL of NaOH (0.1 M). The weight changes in the sample were measured every 20 minutes till constant weight up to a maximum of 140 min. The % swelling (% weight change) was calculated by using the equation below where W_o and W_t are the weights of the microspheres initially [14,15]:

$$\frac{W_t - W_o}{W_o} \times 100$$

8. Ultraviolet Spectroscopy

DU 730 UV-Vis spectrophotometer (Beckman Coulter, USA) was used to characterize the regenerated nanocellulose composites for absorbance and transmittance in the ultraviolet and visible region ranging from 200 to 1000 nm.

9. Scanning Electron Microscopy (SEM)

Surface morphology of the regenerated cellulose nanofibers and metal oxides composites was investigated using Phenom ProX Scanning Electron Microscopy, USA. Before the analysis, the composites were sputtered with thin gold layer to avoid electrostatic charging during examination. The micrographs with a magnification of 500 times were obtained by back scattered electron detector (BSE) in order to register both topography and compositional contrast.

10. Fourier Transform Infrared (FTIR)

The functional groups in the regenerated nanocellulose, TiO_2 and ZnO composite treatment were analyzed by using the Agilent Cary 630 FTIR spectrophotometer, USA in the range of 400-4,000 cm^{-1} in transmittance mode.

11. X-ray Diffraction (XRD)

Crystal structure of the regenerated nanocellulose composites was determined by X-ray diffraction on a Bruker Nanostar diffractometer, USA (MoKα radiation, λ=0.71073 Å) operating at

45 kV voltage and 40 mA current.

12. Particle Size Analysis

The average size of the regenerated nanocellulose was determined by particle size analyzer Horiba, sz100 at the central Laboratory of the Federal University of Technology, Minna, Nigeria.

13. Preparation of Regenerated Nanocellulose/TiO_2/ZnO Composite and Drug Microspheres

The microencapsulation method was used. The regenerated nanocellulose-metal oxides composite and the tramadol hydrochloride drug were dissolved in dichloromethane at various drug-polymer composite ratios. The organic dispersion was emulsified by mixing into an aqueous external phase containing Tween-20 at room temperature. The emulsion was continuously stirred until the dichloromethane had evaporated. The drug microsphere obtained was filtered and repeatedly washed with distilled water and dried overnight in an oven drier at 40 °C [16-19].

14. Hydration (Swelling) Studies

These studies investigated the maximum time required for the microspheres to completely hydrate and their maximum swelling capacity in phosphate buffer solution. The buffer was prepared by the addition of 100 mL of KH_2SO_4 (0.1 M) to 13 mL of NaOH (0.1 M). The weight changes in the sample were measured every 20 minutes till constant weight up to a maximum of 140 min and the data plotted as weight change versus time. The % swelling (% weight change) was calculated by using the equation below where W_0 and W_t are the weights of the lyophilized wafer initially [20,21]:

$$\frac{W_t - W_o}{W_o} \times 100\%$$

15. Drug Loading

A sample of 1 g of dried regenerated nanocellulose-metal oxide composite and drug microsphere was powdered and 100 mL of a 0.07 M HCL solution was added gradually. The resulting sample was analyzed spectrophotometrically for absorbance [22].

16. Determination of Drug Content

To determine the drug content, an equivalent amount of drug loaded microsphere, which contained 50 mg of drug, was weighed accurately, transferred and stirred for three hours by using a magnetic stirrer. The resultant solution was filtered and the amount of the drug in the filtrate was estimated after suitable dilution prior to ultraviolet (UV) spectrophotometric measurements at 273 nm for tramadol hydrochloride [18].

17. Drug Entrapment Efficiency

In the determination of the drug entrapment efficiency (DEE), an equivalent amount of drug loaded microsphere which contained 50 mg of drug for each composite was taken for evaluation. The weighted microspheres were dissolved in 10 ml dichloromethane in a separating funnel, and the drug was repeatedly extracted with aliquots of 0.1 N NaOH. The extract was transferred to a 100 mL volumetric flask and the volume was made up using 0.1 N NaOH. The solution was filtered and the absorbance was measured against 0.1 N NaOH as blank [16,18,19]. The amount of drug entrapped in the microspheres was calculated by the following formula:

$$\text{DEE\%} = \frac{\text{Actual Drug Content}}{\text{Theoretical drug Content}} * 100$$

18. Drug Release Kinetics

Drug release studies were conducted by means of an orbital shaker. A 50 mg of each accurately weighed formulation was transferred into 250 ml conical flask containing 50 ml phosphate buffer (pH=7.4). They were kept in the shaker at 100 rpm maintained at 37 °C. Aliquots of 1 ml buffer were withdrawn at predefined time intervals and the medium was replaced with the same volume of buffer. The withdrawn samples were centrifuged for 15 minutes and the supernatant sample was collected. This study was carried out for 12 hrs, and the concentration of drug release was estimated by determining the absorbance using a UV spectrophotometer at 273 nm for tramadol hydrochloride. The zero-order, first-order, Higuchi and Korsmeyer-Peppas plots were used to test the drug release mechanism [21,23-25].

RESULTS AND DISCUSSION

1. Physicochemical Studies

Generally, the properties which affect the performance of composites for drug delivery functions include crosslinking effects, the nature of surface functional groups, pore size of the composite material and the form of interactions between the composites. The major reason for the variation of the metal oxides in the composites used is to optimize and ascertain how interactions between ZnO and TiO_2 can affect the drug delivery potentials of nanocellulose.

As shown in Table 2, the moisture content decreases as the proportion of nanocellulose decreases within the composite; this is due to the decrease in the moisture absorbing capability of the composite as a result of a corresponding decrease in the cellulosic components present. The pH remained fairly constant around 6.8 and 6.7 while the degree of crystallinity decreased for the composite as the zinc oxides and titanium oxides, which increased dispersion of the medium increases.

2. Particle size Analysis

The particle size analysis helps to confirm the dimension of the regenerated cellulosic biopolymer. Fig. 1 shows the average particle size of the regenerated nanocellulose as 98.1 nm with well distributed nano-dimensional sizes of the regenerated nanocellulose having a polydispersity index of 0.434.

3. UV Analysis

The absorption peaks of ZnO are due to the electron transition from valence band to the conduction band (*O2p to Zn3d*), while the absorption peaks of TiO_2 are a result of electron jump from non-bonding states of (*O2p to Ti3d*) states in the energy structure

Table 2. Physicochemical parameters of regenerated nanocellulose and regenerated nanocellulose composites

Batches	Moisture content	pH	Degree of crystallinity	% Yield
NC	6.1	6.8	83	59.7
RNCC1	5.7	6.7	78	85.7
RNCC2	5.5	6.7	73	88.3
RNCC3	4.9	6.8	74	88.5
RNCC4	5.1	6.7	72	86.5
RNCC5	4.6	6.8	68	87.8

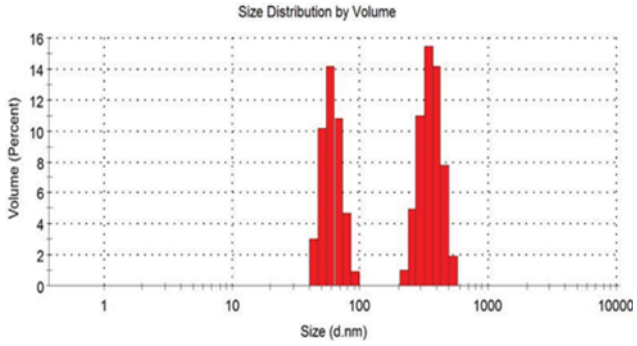

Fig. 1. Particle size of the regenerated nanocellulose.

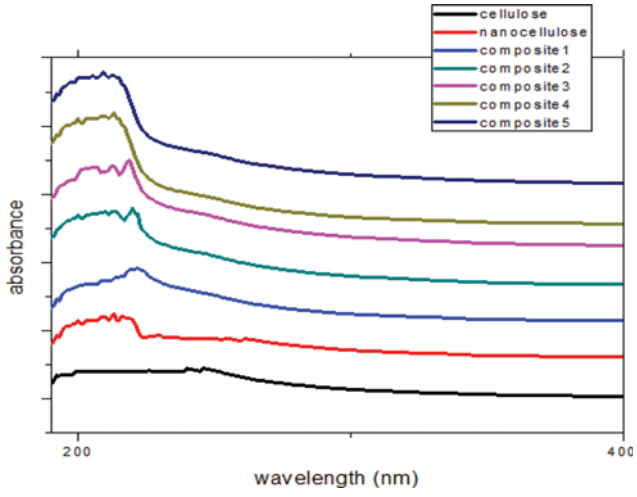

Fig. 2. Absorbance of regenerated nanocellulose composites.

of the nanoparticle. As the interaction between the regenerated nanocellulose, zinc oxide and titanium oxide increased, a noticeable blue shift was observed as shown in Fig. 1 [24-26].

The absorbance values ranged from 3.5819 at 209 nm for the fifth regenerated nanocellulose composite (RNCC5) to 0.8294 at 226 nm for the isolated cellulose. As the mixing ratio increased, the average size of the nanoparticles increased and this led to a decreased dispersion of nanoparticles [27-29]. This tends to reduce the absorbance values of successive regenerated nanocellulose composite with the metal oxides.

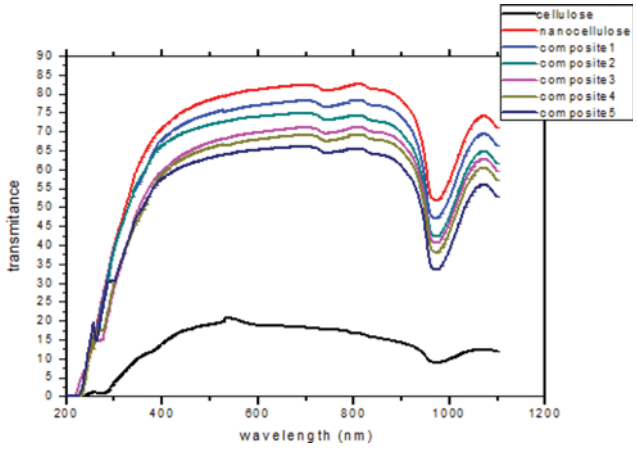

Fig. 3. Transmittance of all regenerated nanocellulose composites.

The transmittance value ranged from 82.54 at 815 nm for regenerated nanocellulose to 20.65 at 538 nm for the isolated cellulose. The degree of aggregation and agglomeration, which increased as particle size and mixing ratio increased after the synthesized composites settled down at the bottom of the container, caused an increase in the transmittance value of the respective composites [30-32].

The transmittance peaks, which were obtained within wavelengths of 538, 815, 817, 694, 815, 811 nm, and 694 nm, respectively, for the regenerated nanocellulose and the metal oxide composites, were a result of the strong scattering power of the RNCC composites formed. The scattering effects in this long wavelength bands of weak UV absorption and non-UV absorption explain the lower transmittance values of the respective composite [33-35].

4. Infrared Analysis

The transmittance peaks at 3,470 and 2,920 cm^{-1} are attributed to -OH and -CH group stretching vibrations for cellulose. The peak at 2,360 cm^{-1} corresponds to the -CH of the C6 of anhydroglucose unit of cellulose, while the peak at 1,639 cm^{-1} shows the presence of residual water in the pore of the cellulose sample. 1,384 cm^{-1} and 1,217 cm^{-1} correspond to the bending vibrations of -CH and C-O, respectively [36]. The small peak at 1,795 cm^{-1} is attributed to the acetyl group of a hemicellulose ester. The transmittance peak at 883 cm^{-1} is assigned to β-glycosidic linkage in cellulose biopolymer, while the one at 1,217 cm^{-1} confirms the C-O-C of the glucopyranose ring of cellulosic cellobiose unit. The peaks at 1,141 cm^{-1} and 1,091 cm^{-1} represent the deformations of C-H rocking vibrations [37].

All the C-H rocking vibrations were overlapped to give a new broad band at 1,222 cm^{-1} while the reduction in intensity of the hydroxyl and -CH stretching vibrations at 3,356 and 2,922 cm^{-1} proves the formation of a crystalline phase of nanocellulose [38]. The absence of a visible peak at the carbonyl region confirms the absence of coumaric esters from lignin unit, while the peak at 883 cm^{-1} is attributed to the ether band of a glucopyranose for a cellulose nanofiber. From the general overview of the overlapped IR spectra, it can be seen that there were slight wave numbers shift for the functional group as the concentration of TiO_2 and ZnO increases in the composite. The variation for the wavenumber of -OH of cellulose is 3,423-3,426-3,443-3,443-3,441 cm^{-1} for the five composites, respectively, and the -CH wavenumber varies as 2,899-2,901-2,901-2,891-2,891 cm^{-1} for the five composites, respectively. These wavenumbers increased slightly throughout the composites.

The 995-1,000 cm^{-1} band attributed for Ti-O became fairly pronounced as the percentage of titania in the composite increased while the bands from 418 to 426 cm^{-1} is attributed to the stretching vibration band for Zn-O. The shift to higher wavenumbers and peaks became higher and wider due to a strong interaction between oxygen atoms of cellulose nanofiber and the metal oxide particles [7]. The appreciable increase in wavenumbers for the functional group region proves the immobilization of titania and zinc oxide particles in the nanocellulose matrix. The bending vibrations of -CH_2, -CH, C-O, which ranged from 1,435 to 1,317 cm^{-1}

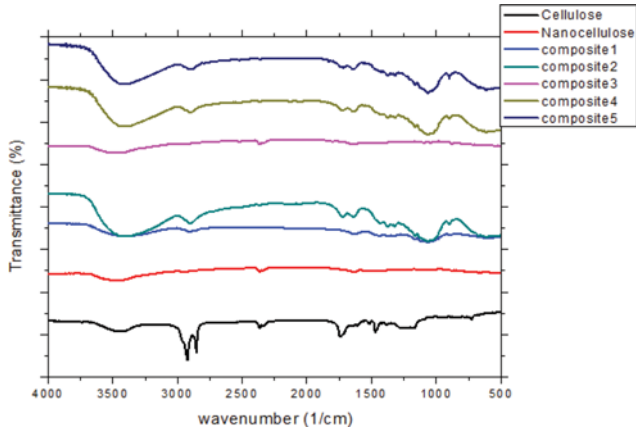

Fig. 4. Infrared spectra for the cellulose, nanocellulose and the composites.

and the -CH rocking vibration which ranged from 1,163 to 1,031 cm^{-1} in the fingerprint region showed a characteristic decrease in wavenumbers [39]. This result revealed that the metal-oxygen bonds created within the composite might have depolarized the -CH and C-O bonds, thereby reducing the wavenumbers.

5. SEM Analysis

The SEM image of the cellulose show bundles of cellulosic fibers standing in isolation in Fig, 5. The irregularly shaped bundles depict the low level of crystallinity of the cellulose isolated. After acid hydrolysis, the cellulosic samples were separated to form a stiff, rod-like strand in Fig. 4. Each strand represents each crystalline domain for the respective cellulose nanofibers.

From the general overview, as the regenerated nanocellulose strands were treated with the metallic oxides, a remarkable decrease in the length of the rod-like strands was observed. It can be concluded that the surface points where the concentration of metal oxides appear highest are the points of fracture. After the compositing, the strands are bound together and the TiO_2 and ZnO particles are anchored on the surface of the nanocellulosic fibers at the early stage of compositing. The closeness of the strands after compositing might be due to dispersion forces generated by the metal oxide orbitals. The metal oxides are found on the surface at the early stage of compositing. This shows that the hydroxyl groups on the nanocellulose fibers tend to immobilize and stabilize the metal oxides.

At the fourth and fifth stage of compositing, the regenerated nanocellulose composite becomes well entangled into an irregularly aligned bunch with significant cavities. This shows that the metal oxides found their way into the pores of the regenerated nanocellulose as the reaction continued. This is further supported by the fact that the metal oxides were no more concentrated at the surface of the regenerated nanocellulose even at high concentration.

6. X-ray Diffraction

From Fig. 7 the XRD pattern of the nanocellulose with JCPDS number of 056-1718 shows characteristic peaks at angle 2θ of 16.6°, 22.7° and 34.4° which represent 110, 200 and 004 planes of crystalline phase of nanocellulose with monoclinic structure [40]. The appearance of peaks at 17.5°, 24.5°, and 32° reveals the hexagonal wurtzite structure of ZnO, while the peaks at 25.4°, 38°, 48.3°, 53.8° show the presence of TiO_2 (21-1272) The crystallinity of the nanocellulose decreases with doping with ZnO and TiO_2 and the peaks decrease as the amount of TiO_2 and ZnO increases due to crystal size and crystallinity increase [7]. The 220 plane of ZnO vanishes as the amount of ZnO increases and no new peaks are observed during and after compositing to confirm that no other phase is present. No prominent change in the crystalline region of nanocellulose shows that the penetration of TiO_2 and ZnO probably occurred in the amorphous region, though the addition of ZnO and TiO_2 led to dissappearance of some cellulose peaks [41].

7. Drug loading and Entrapment Efficiency

A decrease in drug loading and drug entrapment efficiency was observed for decrease in polymer concentration from RNCC1 to RNCC5 in the table below. With increasing biopolymer content, more particles of drugs would be coated leading to higher encapsulation efficiency [23,24]; as the drug loading increases, the percentage of drug entrapment increases.

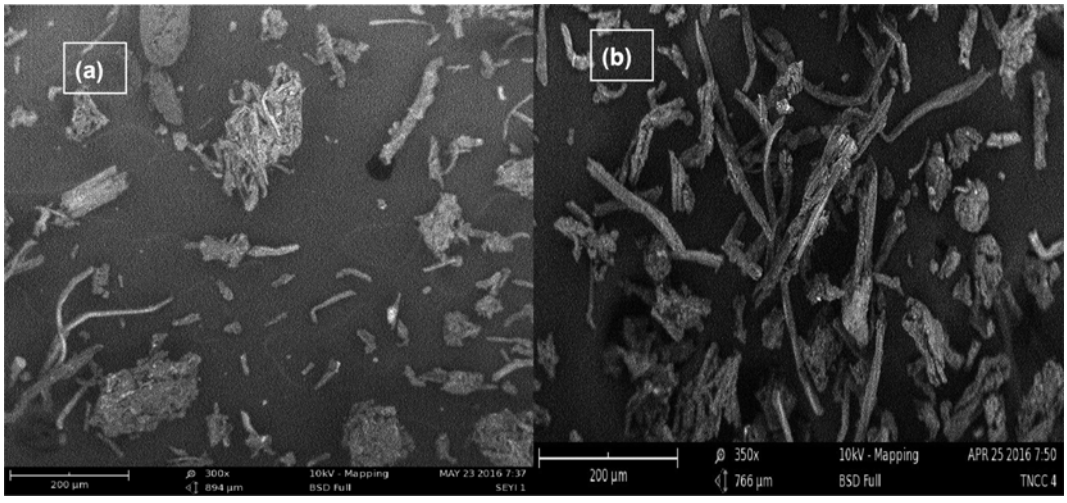

Fig. 5. SEM image of (a) cellulose and (b) nanocellulose.

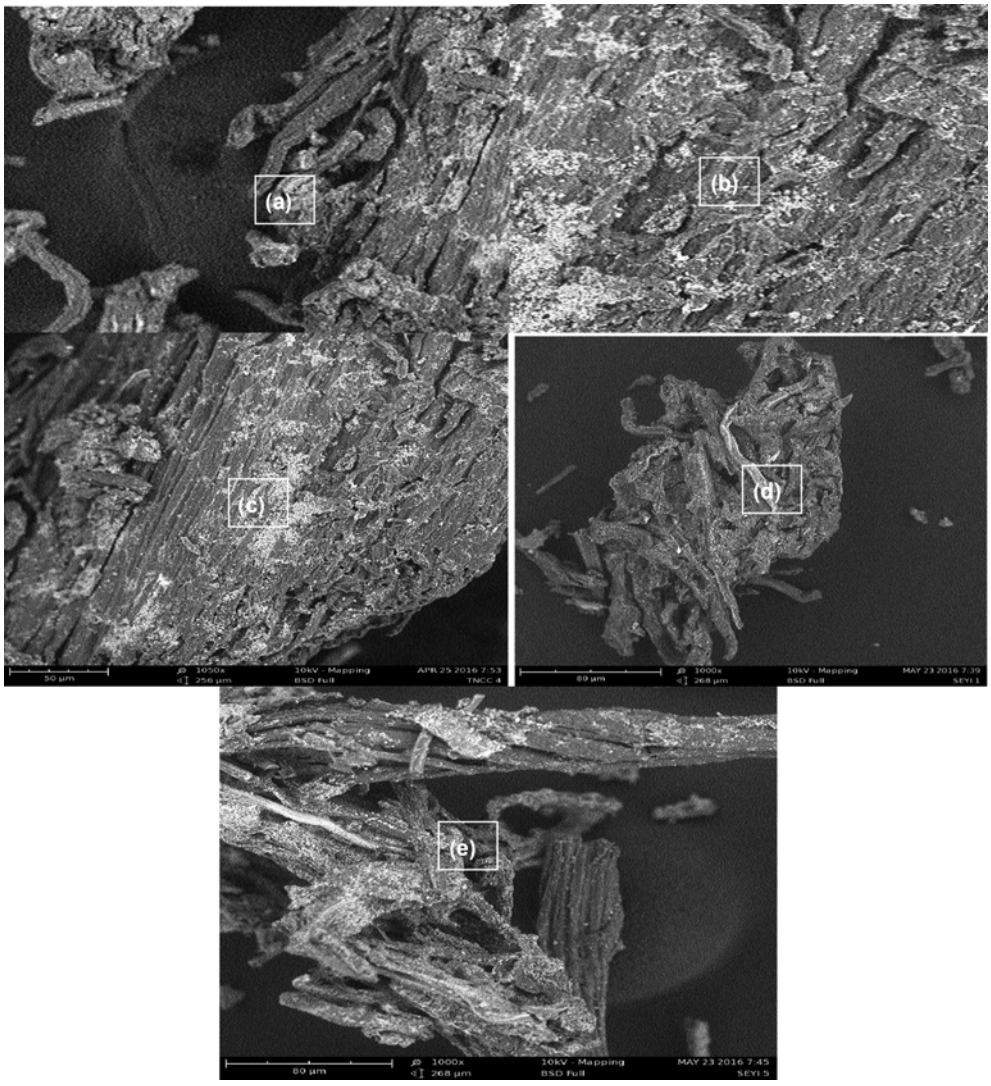

Fig. 6. SEM images of (a) RNCC1 (b) RNCC2 (c) RNCC3 (d) RNCC4 (e) RNCC5.

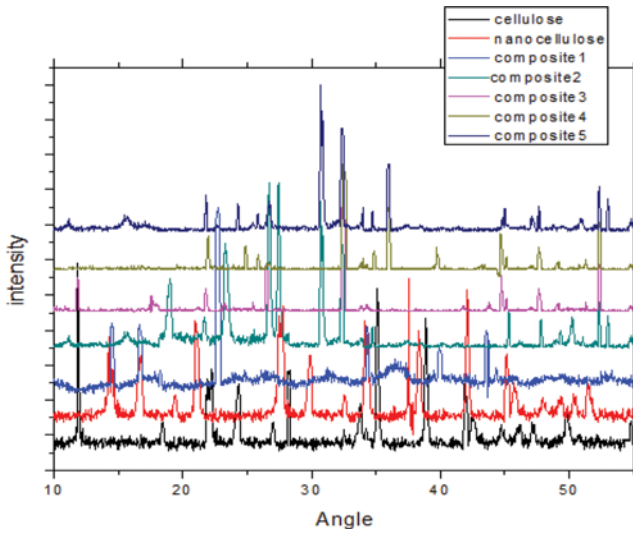

Fig. 7. X-ray diffraction pattern of cellulose, nanocellulose and the composites.

Table 3. Drug loading and entrapment efficiency of tramadol HCl in the composites

Composites	Tramadol hydrochloride	
	Drug loading	Entrapment efficiency
RNCC1	17.9	71.6
RNCC2	18.2	72.8
RNCC3	19.4	77.6
RNCC4	21.1	84.4
RNCC5	21.6	86.4

8. Drug Release Profile

The percentage drug released for the different composites was 97.70%, 97.14%, 92.50%, 88.57% and 92.2% respectively. The composite with the lowest proportion of ZnO and TiO_2 (RNCC1) released the highest percentage of tramadol. Though RNCC1 had a faster initial drug release rate of about 24%, this burst effect was significantly reduced as the proportion of the metallic oxides in-

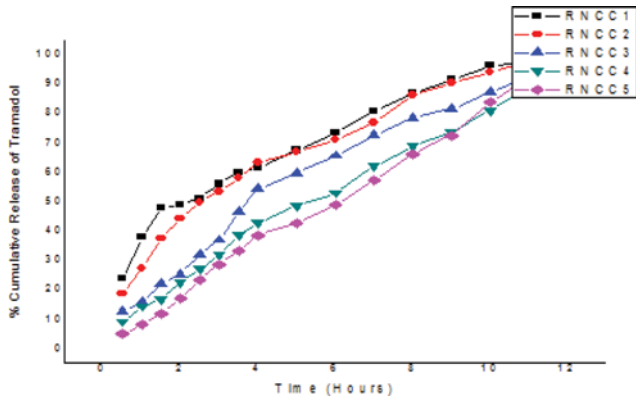

Fig. 8. Percentage cumulative tramadol hydrochloride release profile.

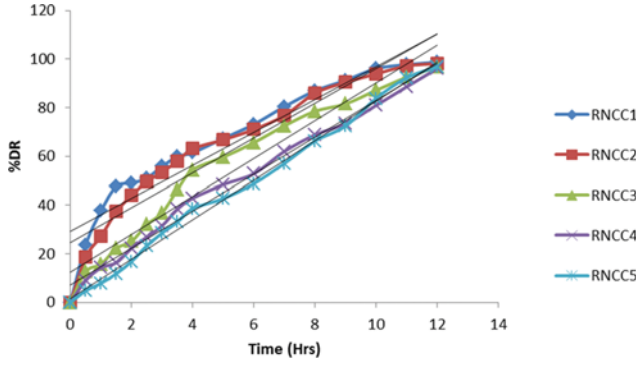

Fig. 9. Zero-order plot for tramadol hydrochloride release.

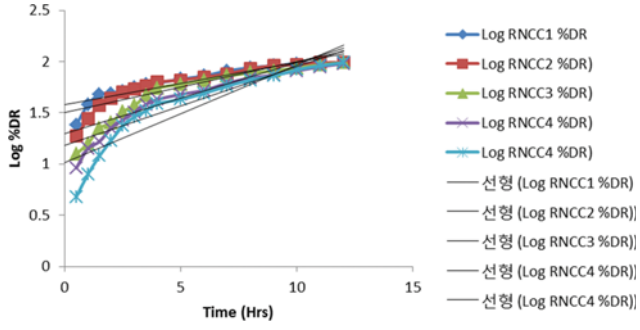

Fig. 10. First-order plot for tramadol hydrochloride release.

creased within the biopolymer composite. As the amount of zinc oxide and titanium oxide increased, the drug release became slow and sustained. The *in vitro* release profile of the formulations pri-

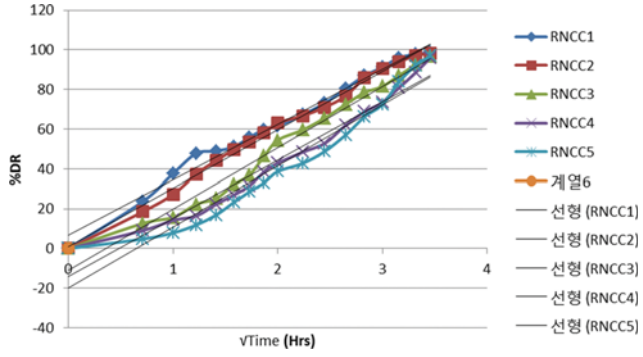

Fig. 11. Higuchi plot for tramadol hydrochloride release.

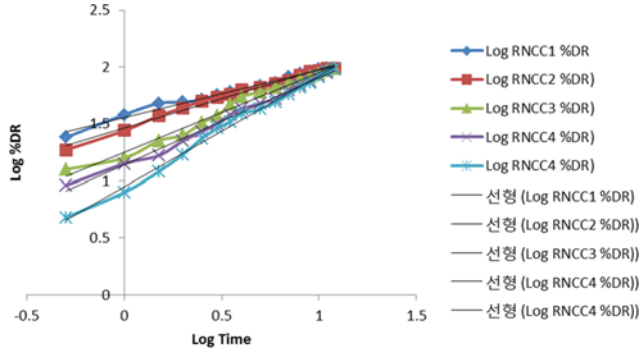

Fig. 12. Korsmeyer-Peppas plot for tramadol hydrochloride release.

marily is dependent on the interactions of the drug with the polymeric network, solubility of the drug, and swelling of the hydrogel in the dissolution media. The release rate was more prolonged as the amount of zinc oxide and titanium oxide increased. The overall slower release was biphasic, i.e., a burst release followed by sustained release. The reason for the sustained drug release as the metallic oxides composition increases may be that as the hydrophobicity of the biopolymer composite increased, the polymer matrix density increased and thus resulting in increased diffusional path length, leading to a decrease in drug release from the microspheres.

9. Drug Release Kinetics

The release kinetics was done to determine the order of the drug release and establish whether the drug release is diffusion- or dissolution controlled and to determine the mode of diffusion. The drug release data was fitted for various kinetic models for zero-order, first-order, Higuchi and Korsmeyer-Peppas plots for all the formulations as shown in the graphs below.

Table 4. Kinetic plot summary for tramadol hydrochloride release

	Zero-order		First-order		Higuchi		Korsmeyer-peppas	
	K	R^2	K	R^2	K	R^2	n	R^2
RNCC1	7.1447	0.9034	0.0952	0.832	29.282	0.9939	0.9704	0.9940
RNCC2	6.7474	0.8840	0.0767	0.8711	27.861	0.9872	0.7018	0.9832
RNCC3	7.7824	0.9570	0.0692	0.8314	30.768	0.9798	0.7637	0.9941
RNCC4	8.0944	0.9957	0.0494	0.7918	30.736	0.9404	0.5145	0.9895
RNCC5	7.5695	0.9894	0.0411	0.8239	29.224	0.9660	0.4188	0.9831

The percentage cumulative tramadol hydrochloride released was subjected to different kinetic models. The drug release profile fitted most for Korsmeyer-Peppas with R^2 value ranging from 0.9831 to 0.9941 and 'n' value, which ranges from 0.4188 to 0.9704 [42]. The Korsmeyer-Peppas model shows that the mechanism of drug release tends to diffusion (Case I) as the composition of zinc oxide and titanium oxide in the nanocellulose biopolymer increases. This 'n' value of 0.4188 for RNCC1 and 0-5145 for RNCC2 confirms this diffusion trend. At higher 'n' value, the delivery mechanism is by both diffusion and erosion. The diffusion-controlled tramadol release is further confirmed with the Higuchi plot, which also has high R^2 value compared to the zero- and first-order plots. The diffusion-controlled tramadol release is further confirmed with the Higuchi plot which also has high R^2 value compared to the zero- and first-order plots.

CONCLUSION

New functional composite materials based on regenerated nanocellulose, titania and zinc oxide were successfully synthesized. The composite material contains titania and zinc oxide strongly bound, which optimizes its hydrophobic content for a better performance in the delivery of tramadol HCl. The results of SEM demonstrate that the titania and zinc oxide are uniformly distributed within the cellulose nanofiber films. IR and UV-Vis spectroscopies confirm that titania and zinc oxide bind to the regenerated nanocellulose.

REFERENCES

1. H. Wang, T. Lin, G. Zhu, H. Yin, X. Lü, Y. Li and F. Huang, *Catal. Commun.*, **60**, 55 (2015).
2. N. Jones, B. Ray, K. T. Ranjit and A. C. Manna, *Microbiol. Lett.*, **279**(1), 71 (2008).
3. Y. Djaoued, S. Balaji and N. Beaudoin, *J. Sol-Gel Sci. Technol.*, **65**(3), 374 (2013).
4. D. M. Tobaldi, R. C. Pullar, A. F. Gualtieri, M. P. Seabra and J. A. Labrincha, *Acta Materialia*, **61**(15), 5571 (2013).
5. H. Wang, T. Lin, G. Zhu, H. Yin, X. Lü, Y. Li and F. Huang, *Catal. Commun.*, **60**, 55 (2015).
6. C. Schutz, J. Sort, Z. Bacsik, V. Oliynyk and E. Pellicer, *Nanoparticle Hybrids*, **7**(10), e45828 (2012).
7. S. Azizi, M. B. Ahmad, M. Z. Hussein and N. A. Ibrahim, *Molecules*, **18**, 6269 (2013).
8. A. Snyder, Z. Bo, R. Moon, J. Rochet and L. Stanciu, *J. Colloid Interface Sci.*, **399**, 92 (2012).
9. S. B. Tiwari, T. K. Murthy, M. Raveendra Pai, P. R. Mehta and P. B. Chowdary, *AAPS PharmSciTech.*, **4**(3), 18 (2003).
10. A. Mohan and T. Vaishali, *American J. Adv. Drug Delivery*, **1**(4), 435 (2013).
11. P. Y. Chauhan, R. S. Sapkal, V. S. Sapkal and G. S. Zamre, *Int. J. Chem. Sci.*, **7**(2), 681 (2009).
12. Y. Zhang, C. Liu, S. Wang, Y. Wu, Y. Meng, J. Cui and Z. Zhou, *Wood Fiber Sci.*, **47**(3), 1 (2015).
13. L. Zhang, Y. Jiang, Y. Ding, N. Daskalakis, L. Jeuken, M. Povey, A. J. O'Neill and D. W. York, *J. Nanopart. Res.*, **12**(5), 1625 (2009).
14. F. Kianfar, M. Antonijevic, B. Chowdhry and J. S. Boateng, *Colloids Surf., B Biointerfaces*, **103**, 99 (2013).
15. M. C. Straccia, G. G. Ayal, I. Romano, A. Oliva and P. Laurienzo, *Marine Drugs*, **13**, 2890 (2015).
16. M. Fentie, A. Belete and T. G. Mariam, *J. Nanomedicine Nanotechnol.*, **6**, 262 (2015).
17. T. Sivakumar, P. Venkatesan, R. Manavalan and K. Valliappan, *J. Basic Clinical Pharmacy*, **69**(1), 154 (2007).
18. A. S. Reddy and A. K. Sailaja, *World J. Pharmacy Pharmaceutical Sci.*, **3**(6), 1781 (2014).
19. P. Sudhakar, S. Bhagyamma, S. Siraj, K. Sekharnath, K. Rao and M. Subha, *J. Appl. Pharm. Sci.*, **5**(2), 51 (2015).
20. F. Kianfar, M. Antonijevic, B. Chowdhry and J. S. Boateng, *Colloids Surf. B: Biointerfaces*, **103**, 99 (2013).
21. M. C. Straccia, G. G. Ayal, I. Romano, A. Oliva and P. Laurienzo, *Marine Drugs*., **13**, 2890 (2015).
22. N. Garud and A. Garud, *Tropical J. Pharmaceutical Res.*, **11**(4), 577 (2012).
23. M. Pandey, M. C. I. Mohd Amin, N. Ahmad and M. M. Abeer, *Int. J. Polym. Sci.*, **2013**, 1 (2013).
24. M. M. Ibrahim, Y. Tamer, A. Fahmy, E. I. Salaheldin, F. Mobarak, M. A. Youssef and M. R. Mabrook, *J. American Sci.*, **10**(12), 108 (2014).
25. P. A. Rodnyi and I. V. Khodyuk, *Optics Spectroscopy*, **111**(5), 776 (2011).
26. S. M. Soosen, B. Lekshmi and K. C. George, *ISSN: 0973-7464, SB Academic Review*, **16**(1&2), 57 (2009).
27. H. Kumar and R. Rani, *Int. Lett. Chem., Phys. Astronomy*, **14**, 26 (2013).
28. A. Janotti and C. G. Van de Walle, *Reports on Progress in Physics*, **72**(126501), 29 (2009).
29. L. Qin, C. Shing, S. Sawyer and P. S. Dutta, *Optical Mater.*, **33**, 359 (2011).
30. M. A. Pugachevskii, *Technical Phys. Lett.*, **39**(1), 36 (2013).
31. T. M. Hammad, J. K. Salem and R. G. Harrison, *Rev. Adv. Mater. Sci.*, **22**, 74 (2009).
32. T. A. Egerton, *Molecules*, **19**, 18192 (2011).
33. L. M. Martor Ano, C. J. Stork and Y. V. Li, *J. Cosmetic Dermatology*, **9**, 276 (2010).
34. C. Salas, T. Nypelö, C. Rodriguez-Abreu, C. Carrillo and O. J. Rojas, *Current Opinion in Colloid Interface Sci.*, **19**, 383 (2014).
35. S. B. Pal and J. Dutta, *Nanoscience Nanotechnology-Asia*, **2**, 90 (2012).
36. H. Yang, S. Zhu and N. Pan, *J. Appl. Polym. Sci.*, **92**, 3201 (2004).
37. M. S. Nazir, B. A. Wahjoedi, A. W. Yussof and M. A. Abdulah, *Bioresources*, **8**(2), 2161 (2013).
38. A. Alemdar and M. Sain, *Bioresour. Technol.*, **99**(6), 1664 (2008).
39. K. Saelee, N. Yingkamhaeng, T. Nimchua and P. Sukyai, Extraction and Characterization of cellulose from sugra cane bagasse by using environmental friendly method. The 26th Annual meeting of the Thai Society for Biotechnology and International Conference (2014).
40. A. W. Morawski, E. Kusiak-Nejman, J. Przepiorski, R. Kordala and J. Pernak, *Cellulose*, **20**, 1293 (2013).
41. O. L. Galkina, A. Sycheva, A. Blagodatskiy, G. Kaptay, V. L. Katanaev, G. A. Seisenbaeva, V. G. Kessler and A. V. Agafonov, *J. Surf. Coat. Technol.*, **253**, 171 (2014).
42. Q. Yu, P. Wu, L. Li, T. Liu and L. Zhao, *Green Chem.*, **10**, 1061 (2008).